

PAPER

## Functionalization of silk fibroin through anionic fibroin derived polypeptides

To cite this article: Gabriele Griffanti *et al* 2019 *Biomed. Mater.* **14** 015006

View the [article online](#) for updates and enhancements.

### You may also like

- [Comparative Study on Strength of Foamed Concrete Consisting Hybrid Fiber](#)  
N. Mohamad, Khalidah Aziz, A.A.A. Samad et al.
- [Prevascularized bladder acellular matrix hydrogel/silk fibroin composite scaffolds promote the regeneration of urethra in a rabbit model](#)  
Nailong Cao, Lujie Song, Wenjing Liu et al.
- [Nitrite oxidizing bacteria for water treatment in coastal aquaculture system](#)  
S Noorak, S Rakkhiaw, K Limjirakhajorn et al.



**BREATH BIOPSY**

### Breath Biopsy Panel for Focused Biomarker Discovery in Respiratory Disease Research

Providing high confidence identification of non-invasive breath biomarkers to distinguish, monitor and assess therapeutic responses across a range of chronic inflammatory airway diseases

**WATCH OUR INTRODUCTORY WEBINAR**

# Biomedical Materials



## PAPER

# Functionalization of silk fibroin through anionic fibroin derived polypeptides

RECEIVED  
29 May 2018

REVISED  
22 August 2018

ACCEPTED FOR PUBLICATION  
10 October 2018

PUBLISHED  
12 November 2018

Gabriele Griffanti<sup>1,2</sup> , Mark James-Bhasin<sup>2</sup>, Ilaria Donelli<sup>3</sup>, Giuliano Freddi<sup>3,4</sup> and Showan N Nazhat<sup>2,5</sup> 

<sup>1</sup> Dipartimento di Biotecnologie e Bioscienze, Università degli Studi di Milano—Bicocca, Milano, I-20126, Italy

<sup>2</sup> Department of Mining and Materials Engineering, McGill University, Montréal, QC, H3A 0C5, Canada

<sup>3</sup> Innovhub-SSI, Silk Division, Milano, I-20133, Italy

<sup>4</sup> Present address: Silk Biomaterials, s.r.l., Lomazzo (Como), I-22074, Italy.

<sup>5</sup> Author to whom any correspondence should be addressed.

E-mail: [showan.nazhat@mcgill.ca](mailto:showan.nazhat@mcgill.ca)

**Keywords:** silk fibroin, mineralization, osteoblastic differentiation, electrospinning

Supplementary material for this article is available [online](#)

## Abstract

While silk fibroin (SF)-based fibrous matrices are often considered as templates to mimic the native biomineralization process, their limited ability to induce apatite deposition hinders their potential applications in bone tissue engineering. In this study, it was hypothesized that the incorporation of anionic fibroin derived polypeptides (Cs), generated through the  $\alpha$ -chymotrypsin digestion of SF, into SF would induce apatite deposition. The effect of Cs incorporation and content on the mineralization of fibrous, electrospun (ES) SF matrices, was assessed in simulated body fluid (SBF). Moreover, the potential role of Cs in mediating the proliferation and osteoblastic differentiation of seeded mesenchymal stem cells (MSCs), *in vitro*, was also investigated. Methylene blue staining indicated that the ES SF matrices became increasingly negatively charged with an increase in Cs content. Furthermore, the mechanical properties of the ES SF matrices were modulated through variations in Cs content. Their subsequent immersion in SBF demonstrated rapid mineralization, attributable to the carboxyl groups provided by the negatively charged Cs polypeptides, which served as nucleation sites for apatite deposition. Seeded MSCs attached on all scaffold types with differences observed in metabolic activities when cultured in osteogenic medium. Relative to basal medium, there was an up-regulation of *alkaline phosphatase*, *runt related transcription factor 2* and *osteocalcin* in osteogenic medium (at days 14 and 21). Cell-induced mineralized matrix deposition appeared to be accelerated on Cs incorporated ES SF suggesting an osteoinductive potential of these polypeptides. In sum, the ability to incorporate Cs into SF scaffolds offers promise in bone tissue engineering applications.

## 1. Introduction

The field of bone tissue engineering strives to offer an alternative approach to bone repair, by restoring tissue function through delivery of viable elements and integration into living tissues [1]. Osteoblastic cells from a donor source can be seeded *in vitro* onto biocompatible, degradable scaffolds and implanted into a defect site either immediately or after an optimized culturing period. To this end, the composition and three-dimensional (3D) structure of the initial construct are all critical to success, and ideally these should mimic the native extracellular matrix

(ECM), which is dominated by mineralized collagen fibres [1].

In recent years, proteinaceous silk-based materials have been considered as templates for mimicking biomineralization [2]. The *Bombyx mori* cocoon-derived silk, constituted by two proteins; fibrous silk fibroin (SF), which are enveloped by sericin, a family of glue-like proteins that hold two SF fibres together, thus forming the composite fibres of the cocoon case and protecting the pupa during metamorphosis [3]. It has been demonstrated that silk fibres allow apatite deposition when immersed in body fluid mimicking solutions [2]. Apatite formation is initiated by the complexation of calcium ions with negatively charged

groups, such as the carboxyl groups carried by Asp and Glu found in the amino acidic sequence of sericin [4]. However, sericin has been shown to induce an immune response [5] and is removed from silk for biomedical applications, though this significantly reduces the ability to induce apatite deposition [2]. While the resulting SF can be considered for biomaterial applications attributable to its biocompatibility, controlled degradation *in vitro* and *in vivo* and its peptidic structure that allows the incorporation of macromolecules [6], its ability to spontaneously induce apatite formation within physiological boundaries is significantly reduced [2]. To this end, the incorporation of negatively charged particles represents a strategy to enhance apatite formation. In fact, apatite growth in SF-based biomaterials has been previously demonstrated by incorporating negatively charged groups such as phosphates [7, 8], carboxyl [9], hydroxyl [9] and sulfonic groups [10]. In contrast, the incorporation of positively charged particles such as poly-Lys into SF did not affect the mineralization process [11].

SF is composed of light and heavy chains linked by a disulfide bond and is rich in hydrophobic  $\beta$ -sheet forming blocks linked by small hydrophilic linker segments [12]. The crystalline regions are mainly composed of Gly-X repeats, where X could be Ala, Ser, Tyr or Val, leading to an assembled hydrophobic, strong and tough material [6]. It has been shown that the digestion of an aqueous solution of SF with  $\alpha$ -chymotrypsin generates peptidic fractions (Cp and Cs peptides) of highly regulated chemistries, namely fibroin derived polypeptides (FDPs) [13]. The Cp fraction, composed of hydrophobic peptides that precipitate during hydrolysis, has a Mw of 40 kDa. It is charge-free and composed of the repetitive  $-(\text{Ala-Gly})_n$ -sequences, typical of the crystalline region of SF. The Cs fraction, on the other hand, has Mw between 2 and 10 kDa, is negatively charged and is the result of a complex mixture of water soluble peptides formed by the amorphous regions of SF [4]. Recently, it was demonstrated that the incorporation of the anionic FDPs (Cs peptides) in fibrous dense collagen gel scaffolds accelerated the deposition of apatite when immersed in Kokubo's simulated body fluid (SBF) [13]. In addition, the osteoblastic differentiation of mesenchymal stem cells (MSCs) seeded in 3D within the dense collagen gel scaffold was accelerated in the presence of Cs peptides [14].

In order to develop a functionalized SF-based scaffold for bone tissue engineering applications, in this study, it was hypothesized that the incorporation of Cs peptides into SF would induce apatite deposition and enhance the osteoblastic differentiation of seeded MSCs. Therefore, electrospun (ES) SF fibres, incorporated with different concentrations of Cs, were generated to provide an ECM-like structure [15]. The effect of Cs concentration on the charge, structural, morphological and mechanical properties of the as-made

ES SF matrices was investigated. The mineralization of acellular ES SF matrices was assessed by immersion in SBF [16]. Furthermore, MSC seeded ES SF matrices were cultured in both basal and osteogenic media. The viability, proliferation, expression of genes involved in the osteogenic pathway, and cell-induced mineralized ECM deposition were investigated.

## 2. Materials and methods

### 2.1. Preparation of Cs peptides incorporated ES SF matrices

SF was extracted from *Bombyx mori* cocoons (purchased from the Department of Agriculture and Environment, Council of Research in Agriculture and Analysis of Agriculture Economics, Padova, Italy). Sericin removal from silk was carried out by autoclaving at 120 °C for 15 min, followed by rinsing in distilled deionized water (DIW) [17]. The resulting SF fibres were neutralized and dissolved in a saturated lithium bromide solution (Sigma-Aldrich, Italy) at 60 °C. The 10% (w/v) solution was dialyzed against DIW with D9402 dialysis tubing cellulose membrane (Sigma-Aldrich, Italy), to generate a final SF aqueous solution with concentration of  $\sim 2\%$  (w/v). This solution was then used to prepare solvent cast SF films and to generate FDPs by dissolving  $\alpha$ -chymotrypsin (an enzyme-to-substrate ratio of 1:100) where after 24 h at 37 °C, the supernatant was freeze-dried to recover the soluble peptides (Cs fraction).

The electrospinning of fibrous SF matrices with different Cs concentrations was carried out as previously described [18]. ES SF matrices were prepared by dissolving pre-prepared solvent cast SF films in formic acid (98 vol%, Sigma-Aldrich, Italy) at room temperature under gentle stirring. SF solution at 8% (w/v) was then transferred into a 50 ml syringe and ES via an ad hoc apparatus [19] by applying a flow rate of  $0.8 \text{ ml h}^{-1}$ , an electric field of 15 kV, and an electrode distance of 13 cm for a deposition time of 6 h. For Cs incorporated ES SF matrices, the lyophilized anionic FDPs were added to the spinning solution at 1%, 2%, 5% and 25% (w/w) concentrations to fabricate SF + Cs 1%, SF + Cs 2%, SF + Cs 5% and SF + Cs 25%, respectively, and were compared with neat ES SF matrices. All ES matrices were dried at room temperature under a chemical hood overnight, followed by treatment in methanol for 20 min to increase SF crystallinity [20].

### 2.2. Methylene blue dye binding

The capacity of ES SF and Cs incorporated SF matrices to bind cationic dye (methylene blue, 0.1%; Sigma-Aldrich, Canada) was investigated as an indicator of their electronegativity. Samples were cut into  $1 \text{ cm}^2$  squares and immersed in the dye solution at 37 °C for 30 min, followed by rinsing in DIW. Specimens were

maintained under darkness to prevent dye photobleaching.

### 2.3. Streaming potential

The streaming potential of the ES SF and Cs incorporated SF matrices was measured with an asymmetric clamping cell using an electrokinetic analyzer (Anton Paar, Graz, Austria) [10]. The measurements were performed at room temperature in 10 mM KCl and pH 7.4. Streaming potential measurements were converted into Zeta Potential ( $\zeta$ -potentials) using the modified Smoluchowski-Helmholtz formulation [21].

### 2.4. Mechanical analysis

Tensile testing was carried out on ES SF and Cs incorporated SF matrices ( $n = 4$ ). Specimens (30 mm length, 10 mm width, 0.8 mm thickness) were mounted into the grippers of a Univert tensile testing instrument (CellScale Biomaterials, Canada). Tensile testing was performed with a 10 N load cell and a controlled displacement rate of  $0.1 \text{ mm s}^{-1}$ . The initial load versus displacement data was processed to generate corresponding stress–strain curves. The ultimate tensile strength (UTS) and apparent modulus were calculated as the maximum stress point and the slope of the elastic deformation region, respectively, of the stress–strain curves.

### 2.5. Mineralization in SBF

Kokubo's SBF (1.5X) was prepared as previously described [22] and used to investigate the mineralization potential of the ES SF and Cs incorporated SF matrices. Samples were cut into  $0.5 \text{ cm}^2$  squares and sterilized by immersion in 70% ethanol for 30 min prior to being extensively washed three times with sterile-filtered SBF before immersion in a standardized SBF:protein ratio of 15:1 ( $\text{ml mg}^{-1}$ ) at  $\text{pH } 7.45 \pm 0.02$  and  $37^\circ\text{C}$  for up to 7 d. The solution was replaced at two-day intervals by fresh, sterile-filtered SBF.

### 2.6. Attenuated total reflectance-fourier transform infrared spectroscopy (ATR-FTIR)

ATR-FTIR spectroscopy was used to characterize Cs peptides, ES SF and Cs incorporated SF matrices, as-made, as well as post conditioning in SBF (at days 1, 3 and 7) and cell culture (at day 21). Conditioned samples were washed three times in DIW and freeze-dried for 24 h at  $-104^\circ\text{C}$  and 14 mTorr (BenchTop K freeze-dryer). Spectra were collected (Spectrum 400, Perkin Elmer, USA) using a resolution of  $1 \text{ cm}^{-1}$ , an infrared range of  $4000\text{--}650 \text{ cm}^{-1}$  and 64 scans. Spectra were then corrected with a linear baseline and normalized (absorbance of Amide I at  $1643 \text{ cm}^{-1} = 1.5$ ) using Spectrum software (Perkin Elmer, USA).

### 2.7. Scanning electron microscopy (SEM)

ES SF and Cs incorporated SF matrices as-made, as well as post conditioning in SBF (at days 1, 3, and 7)

and cell culture (at day 21) were morphologically characterized through SEM analysis. Samples were fixed in 4% formaldehyde for 30 min, rinsed with DIW for 10 min and then dehydrated through an ethanol gradient followed by immersion in 1,1,1,3,3,3-hexamethyldisilazane (Sigma-Aldrich, Canada). All analyses were performed on Au/Pd sputter coated samples with a Jeol JSM-7400F scanning electron microscope at 2 kV and 20 mA. Fibre diameters in the ES matrices were quantitatively characterized by image analysis of SEM micrographs. Images were imported into ImageJ (NIH, USA) and the fibre diameters ( $n = 20$  per image) were measured manually to determine their distribution in each ES matrix.

### 2.8. X-ray diffraction (XRD)

XRD was used to investigate the crystal structure of particles deposited on ES SF and Cs incorporated SF matrices. Samples were collected at day 7 in SBF, washed three times in DIW and freeze-dried as described above. The XRD patterns were obtained using a Bruker D8 Discover (Germany), a range from  $6^\circ$  to  $60^\circ$  2-theta degrees at 40 kV and 40 mA. Three frames of  $23^\circ$  were recorded for 9 min and merged during data post processing. The International Centre for Diffraction Data (ICDD) database was used to identify the phase composition.

### 2.9. Culturing of seeded MSCs on Cs incorporated ES SF matrices

Passage 9 *Mus musculus* C57BL/6 bone marrow derived MSCs (Life technologies; Gibco) were incubated at 5%  $\text{CO}_2$  and grown to 80% confluency at  $37^\circ\text{C}$ . The expansion and growth medium consisted of Dulbecco's modified eagle medium (DMEM/F-12) supplemented with 10% foetal bovine serum and  $5 \mu\text{g ml}^{-1}$  gentamicin antibiotic. ES matrices were cut into  $0.5 \text{ cm}^2$  squares and sterilized by immersion in 70% ethanol for 30 min followed by washing three times in sterile phosphate buffered saline. MSCs were plated at a density of  $5 \times 10^3 \text{ cells cm}^{-2}$  on the ES matrices which were then transferred into 24-well plates. Culturing was carried out in either growth medium (basal medium) or in osteogenic differentiation medium that consisted of DMEM/F-12 supplemented with  $50 \mu\text{g ml}^{-1}$  of ascorbic acid, 40 mM of  $\beta$ -glycerophosphate and 10 nM of dexamethasone for up to 21 days. Cell media were replaced at two-day intervals.

### 2.10. Seeded MSC viability

Confocal laser scanning microscopy (CLSM; Carl Zeiss LSM510) was used to image viability and morphology of seeded MSCs at days 1, 7, 14 and 21 in culture. Seeded cells were stained with  $3 \mu\text{M}$  calcein AM solution (i.e. in culture media) and incubated at  $37^\circ\text{C}$  for 15 min prior to viewing. Excitation and emission wavelengths of 490 and 530 nm were used to

visualize the stained cells by plane scanning. The resulting emissions from the stain were detected for image assembly.

### 2.11. Seeded MSC metabolic activity

The alamarBlue<sup>®</sup> assay (Life Technologies, Canada) was used to investigate the metabolic activity of seeded MSCs as an indicator of cell viability and proliferation [23]. ES matrices were stained in growth medium with 10% alamarBlue<sup>®</sup> reagent and incubated for 4 h under darkness in 5% CO<sub>2</sub> and 37 °C. A fluorescent detection system was employed using a TECAN 9600 epifluorescent plate reader with excitation at 530 and 590 nm for emission detection. Analysis was carried out at days 1, 7, 14, and 21 and plotted against the fluorescent intensity, which was proportional to the magnitude of metabolic activity. Data were normalized against fluorescent intensity at day 1.

### 2.12. Seeded MSC gene expression

Quantitative polymerase chain reaction (q-PCR) was conducted to amplify *alkaline phosphatase (Alp)*, *Runx-related transcription factor 2 (Runx2)*, and *osteocalcin (Ocn)* transcripts as indicators of the osteogenic differentiation of seeded MSCs. Samples cultured in both basal and osteogenic media were subjected to the PureLink<sup>®</sup> RNA kit (Life Technologies, Canada). This generated RNA transcripts that were reverse transcribed to cDNA by 200 U  $\mu\text{l}^{-1}$  M-MuLV reverse transcriptase (NEB, USA) in a solution containing 10X reaction buffer, 2.5 mM of each deoxynucleotide triphosphate (NEB, USA), RNase inhibitor at 10 U  $\mu\text{L}^{-1}$ , total RNA transcripts in water, and 50  $\mu\text{M}$  oligo d(T). The reverse transcription reaction underwent incubation at 37 °C for 1 h and the temperature was increased to 50 °C upon completion to denature the reverse transcriptase. SYBR<sup>®</sup> Select (Life Technologies) q-PCR master mix and primer pairs: *Alp* forward: 5'-GGG AGA TGG TAT GGG CGT CT-3', reverse: 5'-AGG GCC ACA AAG GGG AAT TT-3'; *Runx2* forward: 5'-ATC CCC ATC CAT CCA CTC CA-3', reverse: 5'-CTG TCT GTG CCT TCT GGG TT-3'; *Ocn* forward: 5'-GAC AAA GCC TTC ATG TCC AAG C-3', reverse: 5'-AGC AGG GTC AAG CTC ACA TAG-3'; *Gapdh* forward: 5'-AAG GGC TCA TGA CCA CAG TC-3', reverse: 5'-CAG GGA TGA TGT TCT GGG CA-3' (200 nM each) were prepared for entry into the 7900HT q-PCR thermocycler (Applied Biosystems, USA). Cycling conditions were as follows: an initial denaturation of 95 °C for 10 min, followed by 45 repeats of 95 °C of denaturation for 15 s and an annealing/extension phase of 45 s. Using the 2<sup>- $\Delta\Delta\text{Ct}$</sup>  cycle threshold method, data were normalized to the expression of *Gapdh*.

### 2.13. Statistical analysis

Statistical analysis was carried out using an ordinary one-way ANOVA with a significance level = 0.05.

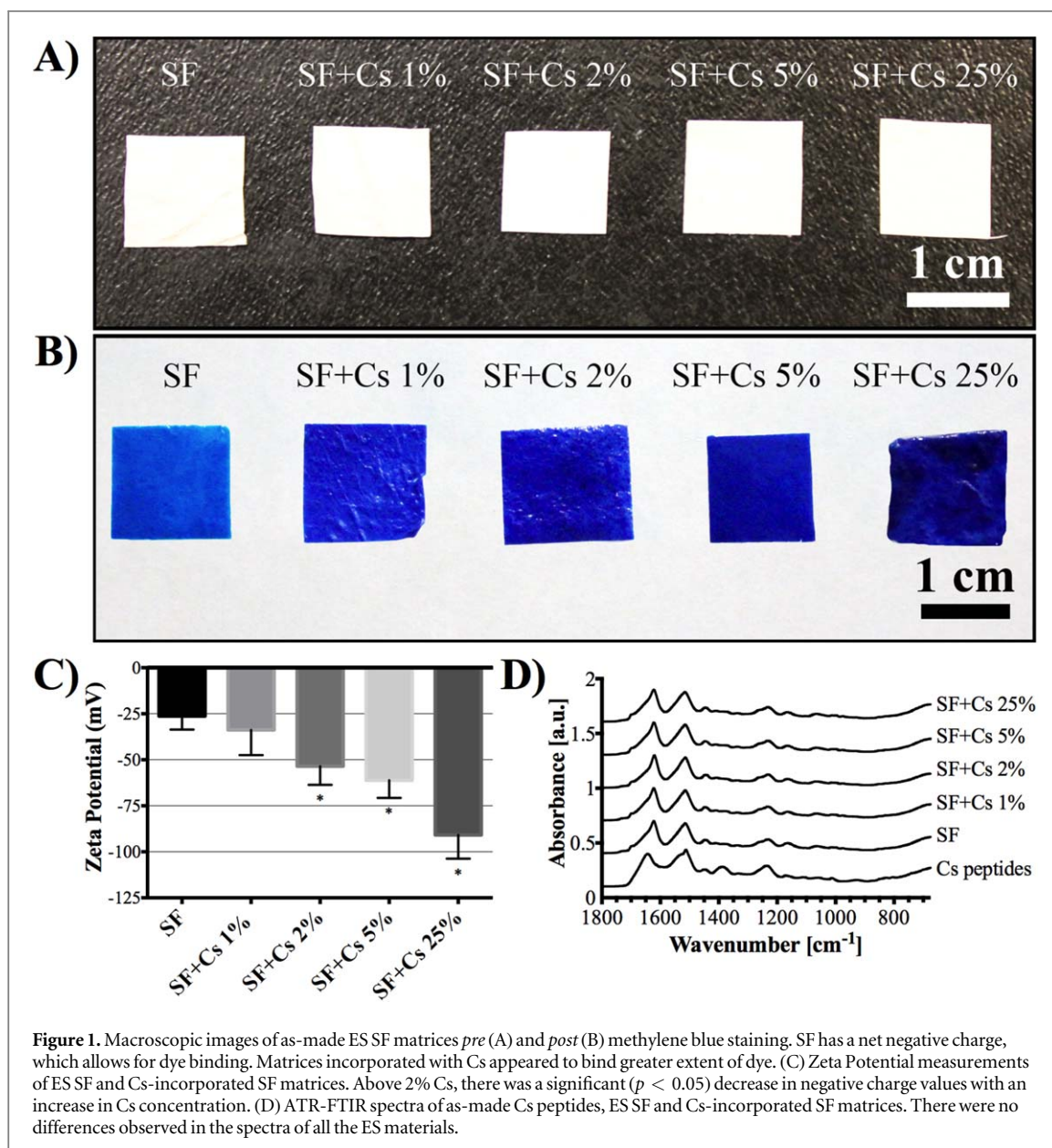
## 3. Results

### 3.1. Characterization of as-made ES SF and Cs incorporated SF matrices

SF matrices were produced by electrospinning solutions with different concentrations of Cs peptides. The incorporation of these anionic FDPs into the various ES SF matrices was confirmed through methylene blue staining (figures 1(A) and (B)). ES SF has the ability to bind the cationic dye due to its net negative charge. Furthermore, there was an increase in colour intensity with Cs content in the matrices. Accordingly, zeta potential analysis showed a decrease in the surface electronegative charge value of the ES SF through Cs incorporation, demonstrating statistically significant effects above 2% incorporation (figure 1(C)). ATR-FTIR spectroscopy allowed for the structural characterization of the as-made materials (figure 1(D)). The spectrum of ES SF is recognized through the two main absorption bands at 1626 and 1517  $\text{cm}^{-1}$  for amide I and II, respectively, revealing its dominant  $\beta$ -sheet conformational structure (figure 1(D)). The spectrum of Cs peptides, on the other hand, revealed that its structure is dominated by random coil conformation through the amide I absorption band at 1643  $\text{cm}^{-1}$ . There were no observed changes in structure through incorporation of different concentrations of Cs peptides. In fact, due to overlapping, the two other main absorption bands found in the Cs peptides spectrum, at 1375 and 1227  $\text{cm}^{-1}$ , corresponding to CH<sub>3</sub> bending absorption and to the amide III absorption bands, respectively, were not observed in the spectra of Cs incorporated SF matrices. SEM micrographs showed no changes in the fibre morphology of ES SF through Cs incorporation (figures 2(A)–(E)). There was no significant difference in fibre diameter of the various matrices, which indicated an average value of approximately 800 nm in all materials (figure 2(F)). The mechanical properties of ES SF, SF + Cs 5% and SF + Cs 25% matrices were evaluated through tensile testing (figure 3). The incorporation of Cs modulated the mechanical properties of ES SF as revealed by the different stress–strain curves of the matrices (figure 3(A)). Compared to the values generated for neat ES SF matrices, the UTS (figure 3(B)) and apparent modulus (figure 3(C)) values significantly increased ( $p < 0.05$ ) in SF + Cs 5% and significantly decreased ( $p < 0.05$ ) in SF + Cs 25% matrices.

### 3.2. Mineralization of ES CF and Cs-peptide incorporated SF in SBF solution

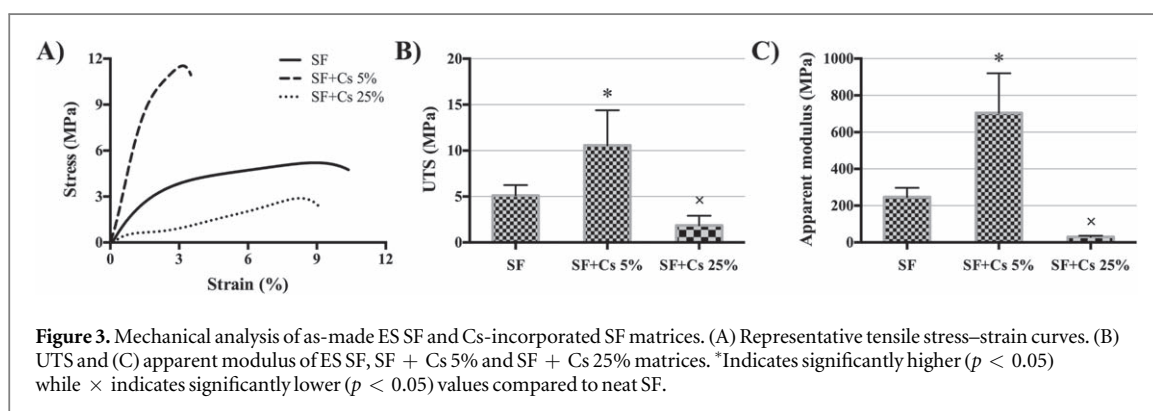
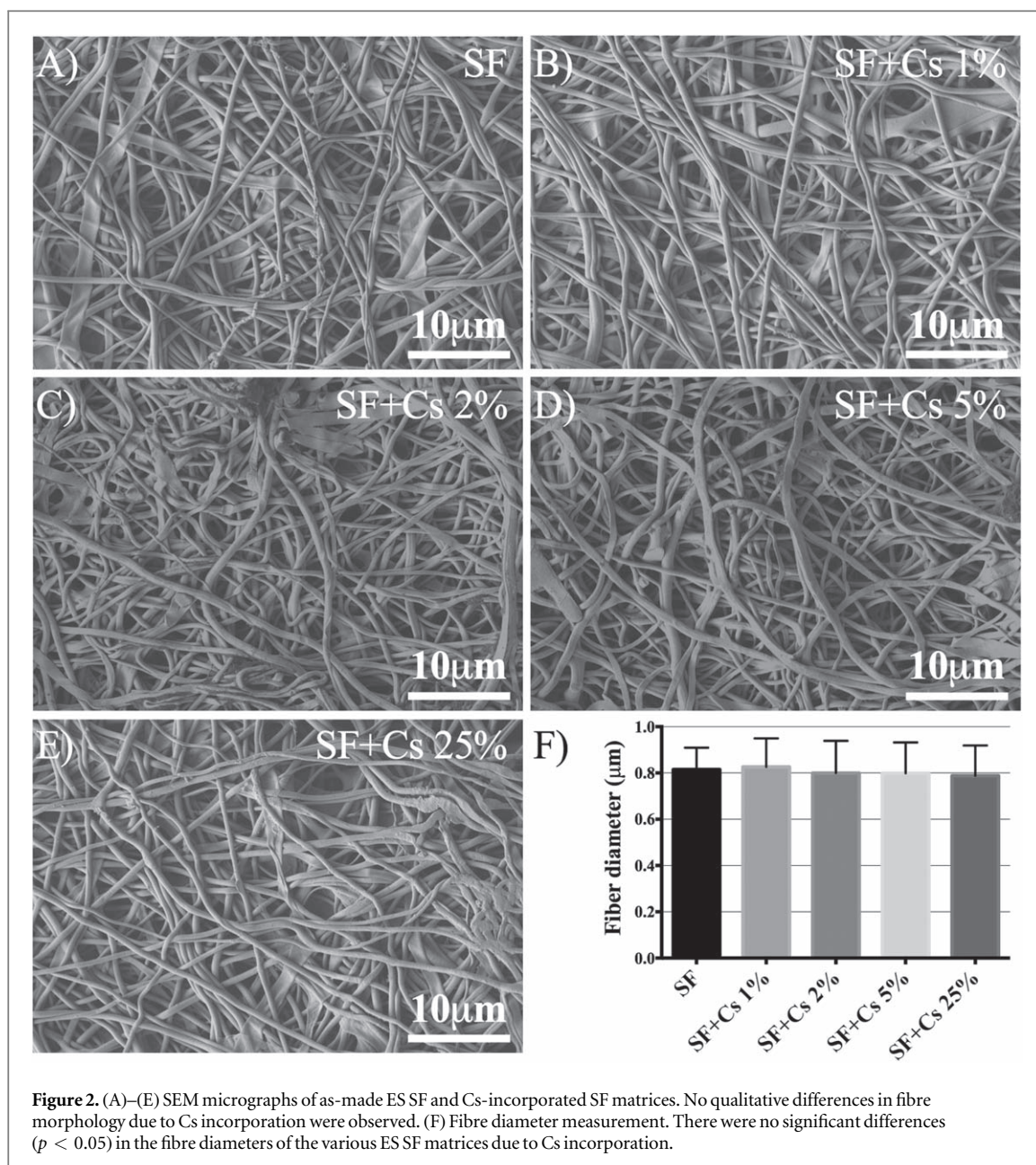
The mineralization of ES SF and Cs-incorporated SF matrices was analysed in 1.5X SBF for up to 7 days. SEM micrographs of Cs-incorporated ES SF matrices showed particle deposition as early as day 1 in SBF (figures 4(Aii–iv); figures S1(B)–(Eii–iv)) is available online at [stacks.iop.org/BMM/14/015006/mmedia](https://stacks.iop.org/BMM/14/015006/mmedia). Qualitatively, particle deposition appeared to increase



with Cs content (figure S1). In contrast, there was no particle deposition observed on ES SF matrix, at all time points (figures 4(Bii) and S1(Aii–iii)). ATR-FTIR spectra of Cs-incorporated SF matrices showed that the absorption bands related to phosphate ( $\nu_1$  at 1070 and 1033  $\text{cm}^{-1}$ ) and carbonate ( $\nu_3$  at 1450 and 1420  $\text{cm}^{-1}$ ) groups, increased with time (figures 4(C) and S2(B)–(E)). Furthermore, at day 7 in SBF, the spectrum of SF + Cs 25% exhibited higher intensities for the absorption bands associated with the phosphate groups compared to those in the other Cs incorporated matrices (figure S2(F)). On the other hand, the spectra of the neat ES SF matrix did not show any differences up to day 7 in SBF (figure S2(A)). XRD diffractograms at day 7 in SBF confirmed that a crystalline phase was present only in matrices incorporated with 5% and 25% Cs peptides (figure 4(D)). Peaks characteristic of apatite pattern, at 32, 47 and 54 2-theta degrees were detected on these matrices.

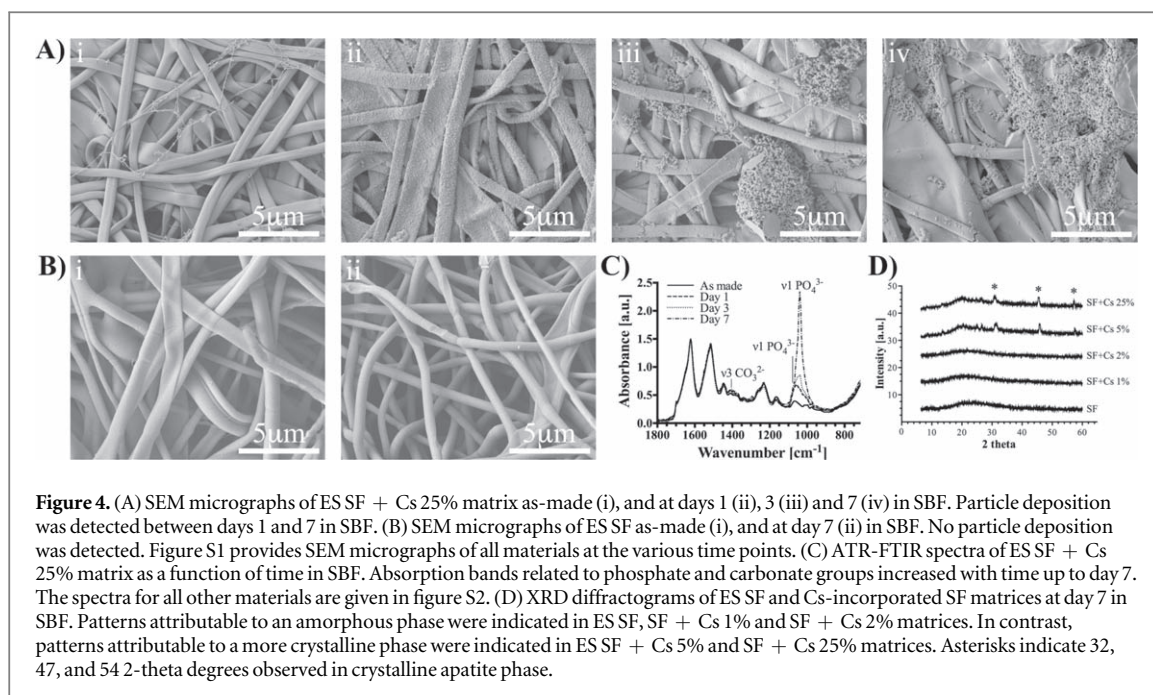
### 3.3. MSC responses to ES SF and Cs-incorporated SF matrices

CLSM of calcein AM stained MSCs at days 1, 7, 14 and 21 demonstrated extensive cell viability on all ES matrices which was not affected by Cs incorporation in ES SF (figure 5). However, a delayed cell growth at day 7 in the SF + Cs 25% matrix in both basal and osteogenic media was observed (figure 5). Cell metabolic activity indicated an increasing trend up to day 14, followed by a decrease at day 21 in both basal (figure 6(A), left) and osteogenic (figure 6(A), right) media. In basal medium, MSC metabolic activity was not affected by Cs incorporation at days 14 and 21 while a significant difference ( $p < 0.05$ ) was observed at day 7 when seeded on the neat ES SF matrix. Under osteogenic medium, MSC metabolic activity was significantly lower ( $p < 0.05$ ) on ES SF matrix at day 7 and higher ( $p < 0.05$ ) on ES SF + Cs 25% matrix at days 14 and 21.



q-PCR analysis at days 14 and 21 assessed the expressions of *Alp*, *Runx2* and *Ocn* as indicators of MSC osteoblastic differentiation (figure 6(B)). The results revealed that while MSCs seeded on all matrices and cultured in osteogenic medium expressed these

markers (figure 6(B) right), only those seeded on the Cs-incorporated SF matrices and cultured in basal medium expressed these markers (figure 5(B), left). At day 21 in osteogenic medium, the level of *Ocn* expression was lower ( $p < 0.05$ ) when MSCs were seeded on



ES SF + Cs 25% matrix (figure 6(B), right). Furthermore, the levels of expression of the three markers were lower ( $p < 0.05$ ) under basal medium at both time points when MSCs were seeded on ES SF matrix (figure 6(B), left). Statistically non-significant fluctuations in the level of expressions of *Alp*, *Runx2* (at days 14 and 21) and *Ocn* (at day 14) were observed in all matrices cultured in osteogenic medium.

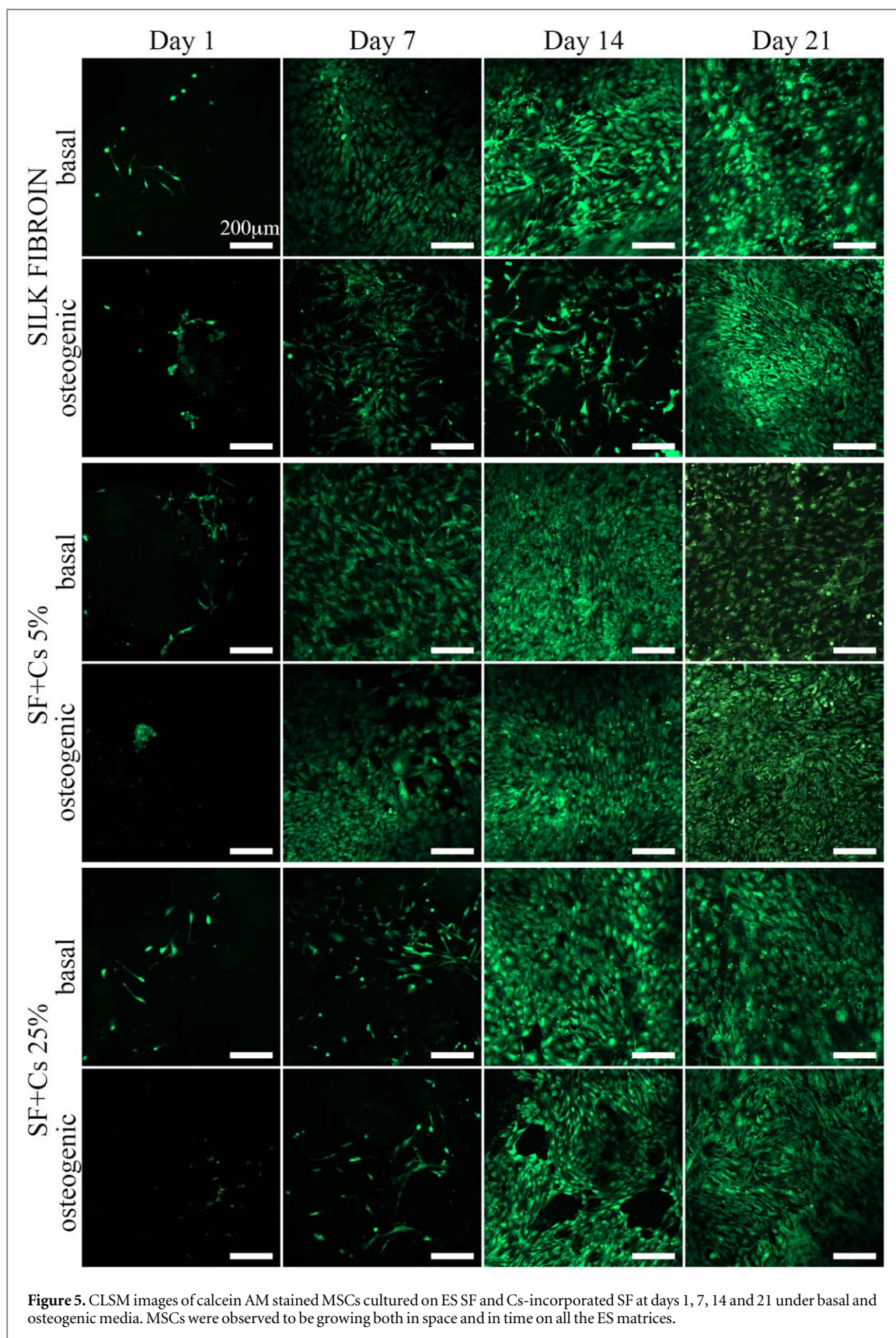
SEM analysis and ATR-FTIR spectroscopy of ES SF matrices in basal and osteogenic media at day 21 were used to assess any mineralized ECM deposition (figure 7). SEM micrographs indicated that cells were anchored and flattened on the ES SF + Cs 25% matrix under osteogenic medium (figures 7(A) and (B), left), corroborating the CLSM images. In addition, there was extensive cell-mediated ECM mineralization on this matrix (figure 7(A), right). In contrast, under the same conditions, the neat ES SF matrix did not display the same level of mineralization (figure 7(B), right). ATR-FTIR spectra did not show any absorption bands related to phosphate or carbonate groups in basal medium (figure 7(C), left), while those in osteogenic medium, indicated increasing absorption bands related to both phosphate and carbonate groups in Cs-incorporated SF matrices and appeared to increase with Cs content (figure 7(C), right). No differences were observed in the spectra of the neat ES SF matrix as-made, acellular and when seeded with MSCs at day 21 in osteogenic medium (figure 7(D), left), suggesting that the unmineralized ECM deposition did not affect the intensity of any of the absorption bands. On the other hand, the absorption bands related to both phosphate and carbonate groups were detected in the spectrum of the MSC-seeded ES SF + 25% matrix (figure 7(D), right). Acellular ES SF matrices at day 21 in both basal (figure S3, left) and osteogenic (figure S3,

right) media did not display any increase in the absorption bands of phosphate and carbonate groups suggesting that the mineral deposition was cell-mediated.

#### 4. Discussion

This study has found that the functionalization of ES fibrous matrices of SF through incorporation of anionic FDPs, represented a promising strategy to template the biomineralization process, as well as to promote the induction of osteogenesis of seeded MSCs. Natural bone is a biocomposite in which inorganic hydroxyapatite nano-crystals are deposited within, and on collagen fibres and arranged into a 3D, hierarchically organised structure [24]. Hydroxyapatite deposition is thought to be controlled by negatively charged noncollagenous proteins with specific binding sites that are carried by acidic amino-acid side chains, such as those rich in Asp [25]. These binding sites interact with calcium and phosphate ions present in physiological fluids in a specific manner to trigger apatite nucleation [25]. Upon their formation, the nuclei spontaneously grow by further addition of calcium and phosphate ions to induce the maturation phase of apatite crystals [25].

Electrospinning is a frequently applied technique in the manufacture of fibrous matrices used in fabricating bone ECM-like structures to template the biomineralization process [26–31]. Matrix fibre diameter, which range from nano-to-microscale dimensions can be controlled by regulating factors, such as solution properties (e.g. pH, concentration and viscosity), electric field strength, and tip-collector distance [32]. Since anionic FDPs are negatively charged [4, 13], and can alter the spinning solution properties, their



addition may affect both the spinning process and resulting fibre dimensions. Nevertheless, it was found that a Cs concentration of up to 25% (w/v) can be successfully incorporated into the spinning solution without altering either the spinning solution properties or

the electrospinning process. For this reason, the morphology and sub-microscale diameter of the resulting fibres in the various Cs-incorporated SF matrices were maintained. However, at higher Cs concentrations, the spinning solution dripped from the

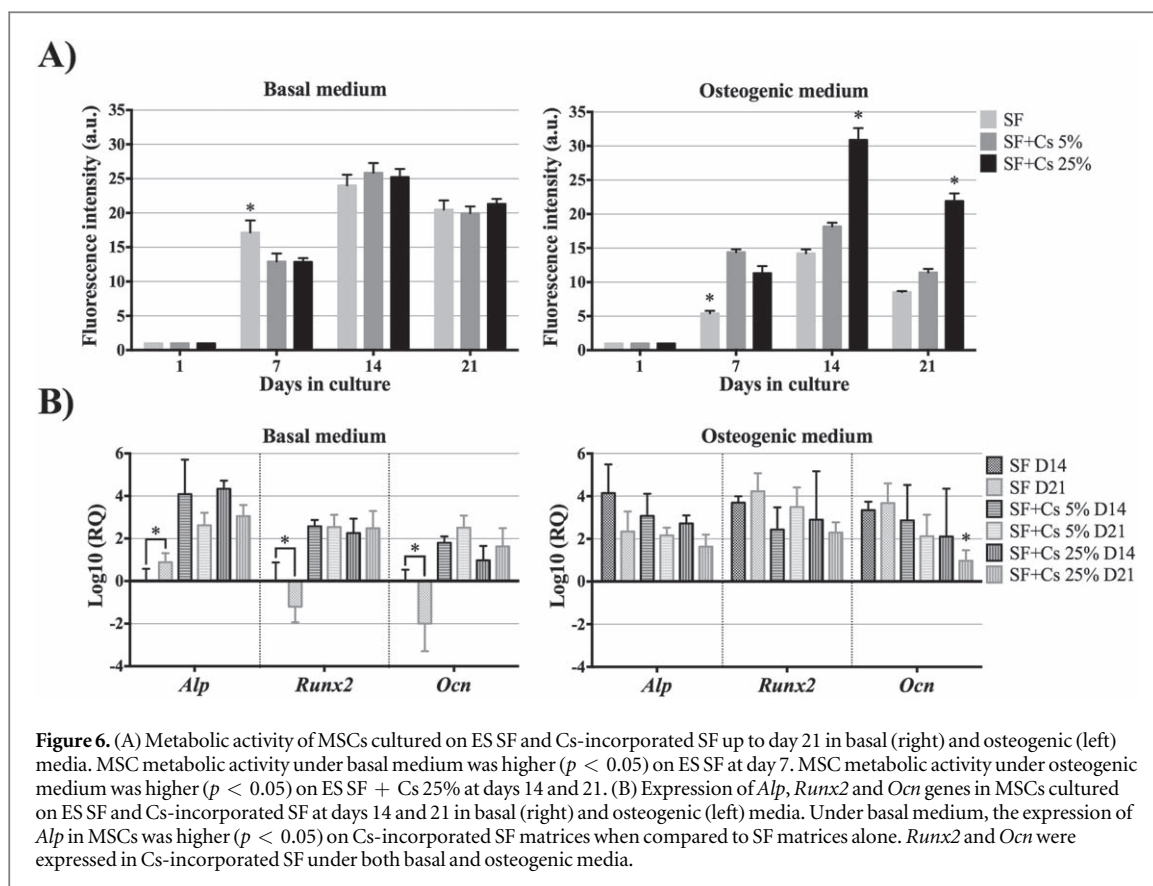


**Figure 6.** (A) Metabolic activity of MSCs cultured on ES SF and Cs-incorporated SF up to day 21 in basal (right) and osteogenic (left) media. MSC metabolic activity under basal medium was higher ( $p < 0.05$ ) on ES SF at day 7. MSC metabolic activity under osteogenic medium was higher ( $p < 0.05$ ) on ES SF + Cs 25% at days 14 and 21. (B) Expression of *Alp*, *Runx2* and *Ocn* genes in MSCs cultured on ES SF and Cs-incorporated SF at days 14 and 21 in basal (right) and osteogenic (left) media. Under basal medium, the expression of *Alp* in MSCs was higher ( $p < 0.05$ ) on Cs-incorporated SF matrices when compared to SF matrices alone. *Runx2* and *Ocn* were expressed in Cs-incorporated SF under both basal and osteogenic media.

spinneret and did not result in fibre formation (data not shown). This may have been due to a drop in dope viscosity with increasing Cs concentration. Methylene blue staining and zeta potential analysis confirmed the net negative charge of the resulting ES SF matrices functionalized with anionic FDPs. Methylene blue staining qualitatively evaluated the successful incorporation of the Cs peptides, which carry an abundance of anionic carboxylic groups that bind the dye [33]. Furthermore, zeta potential analysis quantified the increasing negativity of the matrices of higher Cs content. On the other hand, due to the overlapping of the main absorption bands of Cs and SF, it was difficult to differentiate the impact of Cs incorporation on the overall network structure of SF through FTIR spectroscopy. Tensile testing revealed typical stress-strain curves for ES SF matrices [34, 35], with an initial region characterized by high resistance to deformation (elastic region). This is a result of the cohesive forces generated by the fibre assembly and large number of fibre-to-fibre contact points. After this initial region, a yield point is reached where the modulus gradually decreases as a consequence of fibre slippage (plastic deformation region). The latter region of the stress-strain curve can be observed from the failure point where the fibres failed, resulting in specimen rupture. Interestingly, the incorporation of Cs peptides modulated this profile. SF + Cs 5% showed a higher resistance to deformation followed by a shorter plastic deformation region suggesting a more brittle behaviour compared to SF. This is in line with previously

reported results on the effect of polaxomer 407 incorporation into ES SF. The incorporation of 5% polaxomer 407, an FDA approved compound commonly used to increase the surface hydrophilicity of scaffolds and improve cell attachment, increased the modulus of ES SF [36]. On the other hand, SF + Cs 25% revealed an overall decrease in the mechanical properties. These findings suggested that Cs peptides have a concentration dependent effect on the mechanical properties of the ES matrices.

Immersion of the functionalized ES SF matrices into SBF allowed for the characterization of their mineralization capacity [37]. The incorporation of Cs peptides into ES SF was thought to facilitate the stabilization of calcium-phosphate clusters by forming a structured template where the surface is enriched with the negatively charged Asp and Glu that carry carboxyl groups, which are known to be critical for the heterogeneous nucleation of apatite [8]. This structure aimed to enhance the sequestration of calcium-phosphate nuclei present in the supersaturated solution by forming protein-mineral complexes [38]. The ion complexes are initiated by the strong interactions between  $\text{Ca}^{2+}$  ions and carboxyl groups of the Cs incorporated SF matrices, followed by further interactions with  $\text{PO}_4^{3-}$  ions due to supersaturation effects to form critically sized nuclei that subsequently grow into apatite crystals [39]. This apatite nucleation and growth process appeared to be dependent on Cs peptides concentration. Indeed, XRD diffractograms indicated that an amorphous mineral phase was present on the

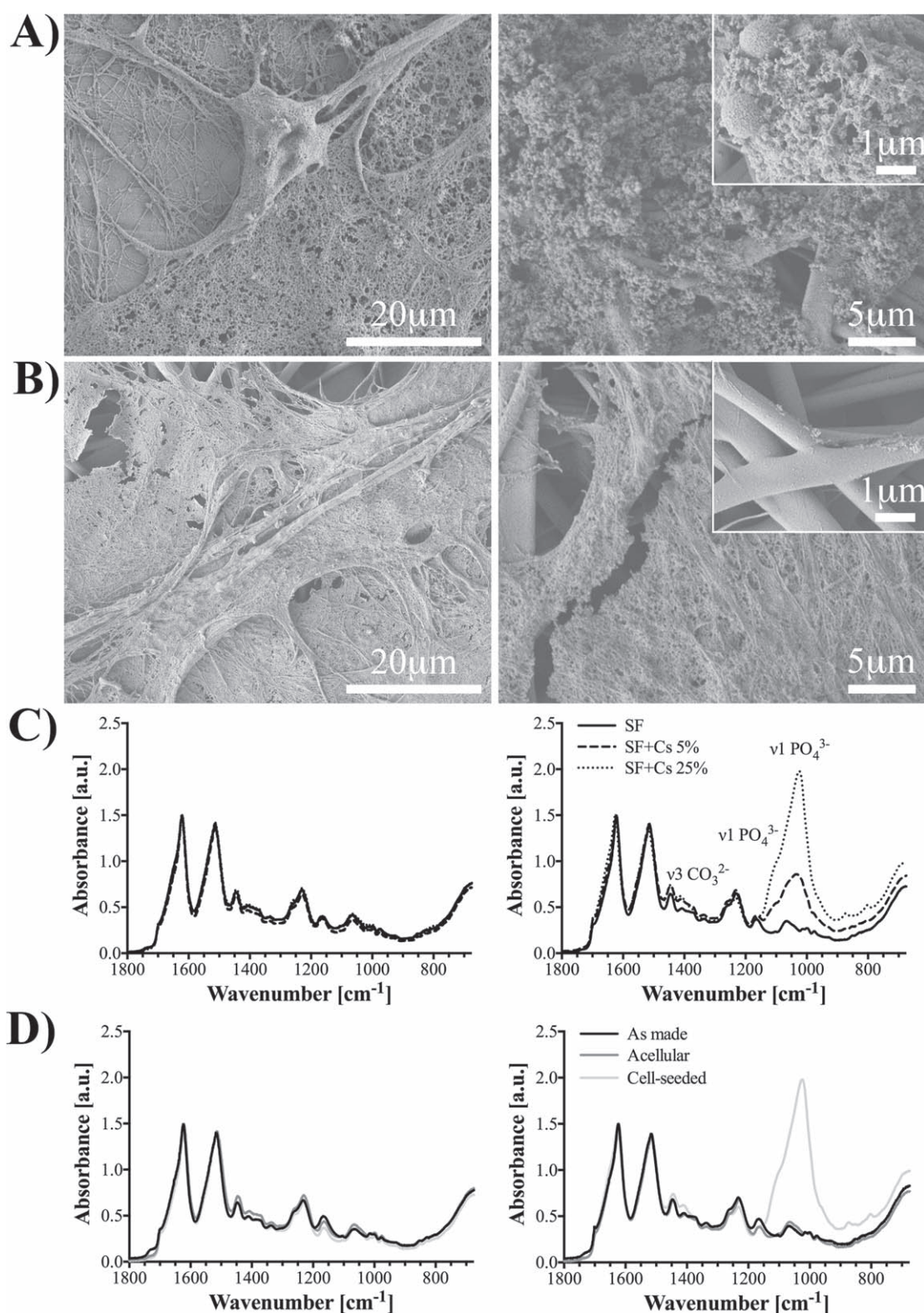


**Figure 7.** (A) SEM micrographs of a cell attached on the surface of the ES SF + Cs 25% matrix through extracellular projections (left). Extensively mineralized cell-deposited ECM on ES SF + Cs 25% in osteogenic medium (right). Insert, higher magnification of mineral particles. (B) SEM micrographs of MSCs cultured on ES SF at day 21 in osteogenic medium (left). ECM deposited on ES SF matrix cultured in osteogenic medium (right). Insert, higher magnification highlighted a minimal deposition of mineral particles. (C) ATR-FTIR spectra of MSC seeded ES SF, SF + Cs 5% and SF + Cs 25% matrices at day 21 in basal (left) and osteogenic (right) media. Absorption bands related to phosphate and carbonate groups were detected in ES SF + Cs 5% and SF + Cs 25% matrices. (D) ATR-FTIR spectra of ES SF (left) and SF + CS 25% (right) matrices as-made and at day 21 in osteogenic medium, acellular and cell-seeded. Only the cell-seeded ES SF + Cs 25% spectrum showed absorption bands associated with phosphate and carbonate groups.

surface of ES matrices functionalized with 1% and 2% Cs peptides. On the other hand, ES matrices functionalized with 5% and 25% Cs peptides displayed a more mature crystalline structure, compatible with that of an apatitic phase [40]. While the deposition of particles reported here were found to be characterized by a morphology consistent with that of apatite crystals observed in previously reported studies of functionalized ES SF [2, 11], the incorporation of Cs-peptides in SF offers advantages. For example, while sericin is known to induce apatite formation, its removal from silk is deemed necessary as it triggers an immune response [2]. However, this results in SF lacking the necessary mineral binding sites which then needs to be taken outside of physiological boundaries to induce mineralization, e.g. through alternate soaking in saturated calcium and phosphate solutions [11].

The creation of a scaffold that both chemically and structurally mimics the native bone ECM is critical in supporting cell adhesion and potentially assisting in new bone formation [41]. The sub-microscale diameter of ES SF fibres mimicked the fibrous ECM components [15] and supported MSC attachment, proliferation and osteogenic differentiation [3]. Osteoinductive molecules are frequently incorporated into SF based materials to improve osteogenic outcomes [25, 42]. Previous approaches have relied on combining the osteoconductive properties of hydroxyapatite particles through their direct incorporation into ES matrices with other osteoinductive molecules such as BMP-2 [42]. Alternatively, the osteoinductive potential of pre-mineralized ES SF on seeded cells has been investigated by incorporating an apatite-binding molecule, Asp, into ES SF matrices to initially induce its deposition, followed by cell seeding [25]. In this study, the osteoinductive effect of anionic FDPs on seeded cells was directly investigated, without a pre-mineralization step, or without coupling with other osteoinductive molecules. MSCs were simply seeded on Cs-incorporated ES SF matrices and cultured in osteogenic medium to investigate any osteoinductive potential of Cs peptides.

MSCs were found to adhere and proliferate on all ES SF matrices. However, the slower rate of cell attachment observed on the ES SF + Cs 25% matrix at day 7 may be due to the modified surface charge as a consequence of Cs peptides incorporation. Accordingly, the metabolic activity of MSCs was slightly reduced by the presence of Cs peptides up to day 7 in basal medium culture. This observation may also be due to the surface wettability of the matrices, which affects cell attachment [43]; i.e. when a material is either too hydrophobic [44] or too hydrophilic [45], protein adsorption is hindered, and consequently, cells cannot attach to the surface of the material [44, 45]. The optimum contact angle value for MSC attachment has been reported to be in the 70° range [46], which is similar to values obtained for ES SF and SF + Cs 5% matrices from contact angle analysis,  $72.13^\circ \pm 3.24^\circ$

and  $71.32^\circ \pm 1.15^\circ$ , respectively, and in line with previous findings on contact angle values for ES SF matrices produced with similar parameters [36]. In contrast, SF + Cs 25% matrix exhibited a greatly increased hydrophilicity to the point that the contact angle analysis could not be performed since, as soon as the water droplet was deposited on the matrix surface, it was immediately adsorbed into the matrix porous structure.

The increase in metabolic activity in MSCs seeded on ES SF matrix cultured in basal medium compared to those cultured in osteogenic medium suggested an increase in proliferation of undifferentiated cells [47], where cells committed to osteoblastic differentiation express a lower proliferation potential [48, 49]. On the other hand, the metabolic activity of cells seeded on ES SF + Cs 25% matrix was higher in osteogenic medium when compared to those cultured in basal medium. Therefore, it can be proposed that the anionic FDPs exhibited a stimulatory effect on cell proliferation similar to that observed with insulin-like growth factor 1 (IGF-1). IGF-1 has been shown to promote both cell proliferation and their mineralization capacity in osteogenic medium thus representing a powerful osteoinductive molecule [50]. Indeed, the expression of genes known to be involved in the osteogenic pathway, even in basal medium, may be attributed to an osteoinductive potential of the Cs peptides. Cs peptides have a net negative charge, which is also a characteristic of noncollagenous binding proteins present in the mineralized tissues, *in vivo* [37]. For this reason, it was postulated that Cs peptides may accelerate the osteoblastic differentiation of seeded MSCs, by mimicking the role of the noncollagenous binding proteins which are known to regulate the osteogenic pathway [37]. *Alp*, an early marker of osteogenesis is related to the pre-osseous cellular metabolism and elaboration of a bone matrix that is chemically mineralizable [51]. *Runx2* is the master osteoblast transcription factor, which regulates numerous genes that determine the osteoblastic phenotype. Therefore, its expression is sufficient to induce the expression of a number of osteogenic markers in non-osteoblastic cells [52]. *Ocn*, a late marker of osteoblastic differentiation pathway, is a tissue specific protein that is secreted only by mature osteoblasts [53]. Interestingly, the level of *Ocn* expression was maintained between days 14 and 21 in ES SF and SF + Cs 5%, but showed a decrease in the case of SF + Cs 25%. Previous studies have reported that the expression of *Ocn* does not change once mineral nodules are formed during the mineralization process [54–57]. However, a decrease in *Ocn* expression has been reported and associated with apoptosis during cell differentiation, where an accelerated differentiation process was shown to increase the number of apoptotic cells [58]. Furthermore, cell death by apoptosis has been reported at advanced stages of mineralization [59]. Indeed, since the extent of mineralization in the cell produced ECM

was more apparent on the ES SF + Cs 25% matrix, it can be hypothesized that the decrease in *Ocn* expression in this matrix was attributable to its advanced mineralization stage thus triggering cell apoptosis and suggesting the accelerated osteoblastic differentiation of MSCs. Furthermore, since the deposition of calcium-phosphate mineral is the terminal stage of the osteoblastic differentiation process [60], this confirms the osteoinductive potential of Cs peptides and echoes previous finding in three dimensional osteoid mimicking dense collagenous scaffolds [14]. However, future investigation on apoptotic markers will be required to confirm this hypothesis.

In sum, the top-down approach in fabricating Cs peptides and incorporation into ES SF provides an interesting alternative to previous reports using other osteoinductive additives [25, 42, 50]. The ability of Cs peptides to induce apatite deposition *in vitro* and accelerate osteogenic outcomes represents a promising approach for bone repair therapies. Follow-up *in vivo* studies will be essential in evaluating the host response to, and the potential osteoinductive properties of, Cs-incorporated SF matrices.

## 5. Conclusions

Fibrous Cs peptide-incorporated SF scaffolds were successfully produced through an electrospinning technique. The incorporation of Cs peptides induced the deposition of apatite on SF matrices, and allowed for the adhesion, proliferation and effectively accelerated the late osteogenic differentiation of seeded MSCs, *in vitro*. Therefore, the incorporation of Cs peptides into SF-based scaffolds holds promise in bone tissue engineering applications.

## Acknowledgments

Funding of CIHR, NSERC, CFI, Quebec MESI, McGill University Faculty of Engineering Gerald Hatch Faculty Fellowship, MEDA and Università degli studi di Milano—Bicocca in collaboration with Assolombarda are gratefully acknowledged. The authors thank Dr Nathalie Tufenkji's group for their assistance with the streaming potential analysis.

## Disclosure

Drs Nazhat and Freddi are named co-inventors on PCT/CA2012/000192, entitled 'Biomaterials, methods for making the biomaterial and uses of the same', which describes the utilization of the silk fibroin polypeptide as a mineralizing, osteoinductive fraction of silk fibroin.

## ORCID iDs

Gabriele Griffanti  <https://orcid.org/0000-0002-6904-9211>

Showan N Nazhat  <https://orcid.org/0000-0002-8134-183X>

## References

- [1] Hutmacher D W 2000 Scaffolds in tissue engineering bone and cartilage *Biomaterials* **21** 2529–43
- [2] Takeuchi A, Ohtsuki C, Miyazaki T, Tanaka H, Yamazaki M and Tanihara M 2003 Deposition of bone-like apatite on silk fiber in a solution that mimics extracellular fluid *J. Biomed. Mater. Res. A* **65** 283–9
- [3] Altman G H, Diaz F, Jakuba C, Calabro T, Horan R L, Chen J, Lu H, Richmond J and Kaplan D L 2003 Silk-based biomaterials *Biomaterials* **24** 401–16
- [4] Freddi G, Faragò S and Maifreni T 1989 HPLC fractionation of Cs peptides of *Bombyx mori* silk fibroin *Sericologia* **29** 307–26
- [5] Wang Z, Zhang Y, Zhang J, Huang L, Liu J, Li Y, Zhang G, Kundu S C and Wang L 2014 Exploring natural silk protein sericin for regenerative medicine: an injectable, photoluminescent, cell-adhesive 3D hydrogel *Sci. Rep.* **4** 7064
- [6] Vepari C and Kaplan D L 2007 Silk as a biomaterial *Prog. Polym. Sci.* **32** 991–1007
- [7] Sato K, Kumagai Y and Tanaka J 2000 Apatite formation on organic monolayers in simulated body environment *J. Biomed. Mater. Res.* **50** 16–20
- [8] Tanahashi M and Matsuda T 1997 Surface functional group dependence on apatite formation on self-assembled monolayers in a simulated body fluid *J. Biomed. Mater. Res.* **34** 305–15
- [9] Tretinnikov O N and Tamada Y 2001 Influence of casting temperature on the near-surface structure and wettability of cast silk fibroin films *Langmuir* **17** 7406–13
- [10] Kawai T, Ohtsuki C, Kamitakahara M, Miyazaki T, Tanihara M, Sakaguchi Y and Konagaya S 2004 Coating of an apatite layer on polyamide films containing sulfonic groups by a biomimetic process *Biomaterials* **25** 4529–34
- [11] Li C, Jin H J, Botsaris G D and Kaplan D L 2005 Silk apatite composites from electrospun fibers *J. Mater. Res.* **20** 3374–84
- [12] Dobb M G, Fraser R D and Macrae T P 1967 The fine structure of silk fibroin *J. Cell Biol.* **32** 289–95
- [13] Marelli B, Ghezzi C E, Alessandrino A, Barralet J E, Freddi G and Nazhat S N 2012 Silk fibroin derived polypeptide-induced biomineralization of collagen *Biomaterials* **33** 102–8
- [14] Marelli B, Ghezzi C E, Alessandrino A, Freddi G and Nazhat S N 2014 Anionic fibroin-derived polypeptides accelerate MSC osteoblastic differentiation in a three-dimensional osteoid-like dense collagen niche *J. Mater. Chem. B* **2** 5339–43
- [15] Ma Z, Kotaki M, Inai R and Ramakrishna S 2005 Potential of nanofiber matrix as tissue-engineering scaffolds *Tissue Eng.* **11** 101–9
- [16] Kokubo T, Kim H M, Kawashita M, Takadama H, Miyazaki T, Uchida M and Nakamura T 2000 Nucleation and growth of apatite on amorphous phases in simulated body fluid *Glass Sci. Technol.: Glastechnische Berichte* **73** (1 Suppl. C) 247–54
- [17] Arai T, Freddi G, Innocenti R and Tsukada M 2004 Biodegradation of bombyx mori silk fibroin fibers and films *J. Appl. Polym. Sci.* **91** 2383–90
- [18] Ghezzi C E, Marelli B, Muja N, Hirota N, Martin J G, Barralet J E, Alessandrino A, Freddi G and Nazhat S N 2011 Mesenchymal stem cell-seeded multilayered dense collagen-silk fibroin hybrid for tissue engineering applications *Biotechnol. J.* **6** 1198–207
- [19] Alessandrino A, Marelli B, Arosio C, Fare S, Tanzi M C and Freddi G 2008 Electrospun silk fibroin mats for tissue engineering *Eng. Life Sci.* **8** 219–25

- [20] Wilson D, Valluzzi R and Kaplan D 2000 Conformational transitions model silk peptides *Biophys. J.* **78** 2690–701
- [21] Walker S L, Bhattacharjee S, Hoek E M V and Elimelech M 2002 A novel asymmetric clamping cell for measuring streaming potential of flat surfaces *Langmuir* **18** 2193–8
- [22] Kokubo T and Takadama H 2006 How useful is SBF in predicting *in vivo* bone bioactivity? *Biomaterials* **27** 2907–15
- [23] Al-Nasiry S, Geusens N, Hanssens M, Luyten C and Pijnenborg R 2007 The use of Alamar blue assay for quantitative analysis of viability, migration and invasion of choriocarcinoma cells *Hum. Reprod.* **22** 1304–9
- [24] Reznikov N, Shahar R and Weiner S 2014 Bone hierarchical structure in three dimensions *Acta Biomater.* **10** 3815–26
- [25] Kim H J, Kim U J, Kim H S, Li C, Wada M, Leisk G G and Kaplan D L 2008 Bone tissue engineering with premineralized silk scaffolds *Bone* **42** 1226–34
- [26] Yoshimoto H, Shin Y M, Terai H and Vacanti J P 2003 A biodegradable nanofiber scaffold by electrospinning and its potential for bone tissue engineering *Biomaterials* **24** 2077–82
- [27] Jang J H, Castano O and Kim H W 2009 Electrospun materials as potential platforms for bone tissue engineering *Adv. Drug. Deliv. Rev.* **61** 1065–83
- [28] Erisken C, Kalyon D M and Wang H 2008 Functionally graded electrospun polycaprolactone and  $\beta$ -tricalcium phosphate nanocomposites for tissue engineering applications *Biomaterials* **29** 4065–73
- [29] Gupta D, Venugopal J, Mitra S, Giri Dev V R and Ramakrishna S 2009 Nanostructured biocomposite substrates by electrospinning and electrospraying for the mineralization of osteoblasts *Biomaterials* **30** 2085–94
- [30] Chen J, Chu B and Hsiao B S 2006 Mineralization of hydroxyapatite in electrospun nanofibrous poly(L-lactic acid) scaffolds *J. Biomed. Mater. Res. A* **79** 307–17
- [31] Venugopal J R, Low S, Choon A T, Kumar A B and Ramakrishna S 2008 Nanobioengineered electrospun composite nanofibers and osteoblasts for bone regeneration *Artif. Organs* **32** 388–97
- [32] Alexander P P P 2016 Scaffolds used for bone tissue regeneration: review *Res. J. Pharm., Biol. Chem. Sci.* **7** 1624–36
- [33] Davidson G F 1947 34—the determination of methylene blue *J. Textile Inst. Trans.* **38** T408–18
- [34] Ohgo K, Zhao C, Kobayashi M and Asakura T 2003 Preparation of non-woven nanofibers of Bombyx mori silk, Samia cynthia ricini silk and recombinant hybrid silk with electrospinning method *Polymer* **44** 841–6
- [35] Ayutsede J, Gandhi M, Sukigara S, Micklus M, Chen H-E and Ko F 2005 Regeneration of Bombyx mori silk by electrospinning: III. Characterization of electrospun nonwoven mat *Polymer* **46** 1625–34
- [36] Kadakia P U, Growney Kalaf E A, Dunn A J, Shornick L P and Sell S A 2017 Comparison of silk fibroin electrospun scaffolds with poloxamer and honey additives for burn wound applications *J. Bioact. Compat. Polym.* **33** 79–94
- [37] George A and Veis A 2008 Phosphorylated proteins and control over apatite nucleation, crystal growth, and inhibition *Chem. Rev.* **108** 4670–93
- [38] He G, Gajjaraman S, Schultz D, Cookson D, Qin C, Butler W T, Hao J and George A 2005 Spatially and temporally controlled biomineralization is facilitated by interaction between self-assembled dentin matrix protein 1 and calcium phosphate nuclei in solution *Biochemistry* **44** 16140–8
- [39] Kong X D, Cui F Z, Wang X M, Zhang M and Zhang W 2004 Silk fibroin regulated mineralization of hydroxyapatite nanocrystals *J. Cryst. Growth* **270** 197–202
- [40] Li C, Vepari C, Jin H-J, Kim H J and Kaplan D L 2006 Electrospun silk-BMP-2 scaffolds for bone tissue engineering *Biomaterials* **27** 3115–24
- [41] Ma P X 2008 Biomimetic materials for tissue engineering *Adv. Drug. Deliv. Rev.* **60** 184–98
- [42] Niu B, Li B, Gu Y, Shen X, Liu Y and Chen L 2017 *In vitro* evaluation of electrospun silk fibroin/nano-hydroxyapatite/BMP-2 scaffolds for bone regeneration *J. Biomater. Sci., Polym. Ed.* **28** 257–70
- [43] Okano T, Yamada N, Sakai H and Sakurai Y 1993 A novel recovery system for cultured cells using plasma-treated polystyrene dishes grafted with poly(N-isopropylacrylamide) *J. Biomed. Mater. Res.* **27** 1243–51
- [44] Colley H E, Mishra G, Scutt A M and McArthur S L 2009 Plasma polymer coatings to support mesenchymal stem cell adhesion, growth and differentiation on variable stiffness silicone elastomers *Plasma Process. Polym.* **6** 831–9
- [45] Lee M, Ko Y G, Lee J B, Park W H, Cho D and Kwon O H 2014 Hydrophobization of silk fibroin nanofibrous membranes by fluorocarbon plasma treatment to modulate cell adhesion and proliferation behavior *Macromol. Res.* **22** 746–52
- [46] Tsuji H, Sommani P, Hattori M, Yamada T, Sato H, Gotoh Y and Ishikawa J 2008 Adhesion patterning of mesenchymal stem cells on polystyrene surface by carbon negative-ion implantation and neuron differentiation on the position *Nucl. Instrum. Methods Phys. Res. B* **266** 3067–70
- [47] Westhrin M, Xie M, Olderooy M Ø, Sikorski P, Strand B L and Standal T 2015 Osteogenic differentiation of human mesenchymal stem cells in mineralized alginate matrices *PLOS One* **10** e0120374
- [48] Malaval L, Liu F, Roche P and Aubin J E 1999 Kinetics of osteoprogenitor proliferation and osteoblast differentiation *in vitro* *J. Cell. Biochem.* **74** 616–27
- [49] Maxson S and Burg K J L 2008 Conditioned media cause increases in select osteogenic and adipogenic differentiation markers in mesenchymal stem cell cultures *J. Tissue Eng. Regen. Med.* **2** 147–54
- [50] Wang S et al 2012 Insulin-like growth factor 1 can promote the osteogenic differentiation and osteogenesis of stem cells from apical papilla *Stem Cell Res.* **8** 346–56
- [51] Orimo H 2010 The mechanism of mineralization and the role of alkaline phosphatase in health and disease *J. Nippon Med. Sch.* **77** 4–12
- [52] Ducey P, Zhang R, Geoffroy V, Ridall A L and Karsenty G 1997 Osf2/Cbfa1: a transcriptional activator of osteoblast differentiation *Cell* **89** 747–54
- [53] Christenson R H 1997 Biochemical markers of bone metabolism: an overview *Clin. Biochem.* **30** 573–93
- [54] Choi J Y, Lee B H, Song K B, Park R W, Kim I S, Sohn K Y, Jo J S and Ryoo H M 1996 Expression patterns of bone-related proteins during osteoblastic differentiation in MC3T3-E1 cells *J. Cell. Biochem.* **61** 609–18
- [55] Bakhty D Z, Wen-Lang L, Pill-Hoon C, Chien Jaro S H-H, Kuber T S and Moon-II C 1998 Differential induction of bone sialoprotein by dexamethasone and osteogenic protein-1 (OP-1, BMP-7) in rat periodontal ligament cells *in vitro* *Int. J. Oral Biol.* **23** 91–101
- [56] Aronow M A, Gerstenfeld L C, Owen T A, Tassinari M S, Stein G S and Lian J B 1990 Factors that promote progressive development of the osteoblast phenotype in cultured fetal rat calvaria cells *J. Cell. Physiol.* **143** 213–21
- [57] Malaval L, Modrowski D, Gupta A K and Aubin J E 1994 Cellular expression of bone-related proteins during *in vitro* osteogenesis in rat bone marrow stromal cell cultures *J. Cell. Physiol.* **158** 555–72
- [58] Choi M H, Noh W C, Park J W, Lee J M and Suh J Y 2011 Gene expression pattern during osteogenic differentiation of human periodontal ligament cells *in vitro* *J. Periodontal Implant Sci.* **41** 167–75
- [59] Lynch M P, Capparelli C, Stein J L, Stein G S and Lian J B 1998 Apoptosis during bone-like tissue development *in vitro* *J. Cell. Biochem.* **68** 31–49
- [60] Panda N N, Biswas A, Pramanik K and Jonnalagadda S 2015 Enhanced osteogenic potential of human mesenchymal stem cells on electrospun nanofibrous scaffolds prepared from eritatar silk fibroin *J. Biomed. Mater. Res. B* **103** 971–82